Observation of Universal Quench Dynamics and Townes Soliton Formation from Modulational Instability in Two-Dimensional Bose Gases

Cheng-An Chen[1] and Chen-Lung Hung[1,2,*]
[1]Department of Physics and Astronomy, Purdue University, West Lafayette, Indiana 47907, USA
[2]Purdue Quantum Science and Engineering Institute, Purdue University, West Lafayette, Indiana 47907, USA

(Received 10 December 2019; accepted 16 November 2020; published 15 December 2020)

We experimentally study universal nonequilibrium dynamics of two-dimensional atomic Bose gases quenched from repulsive to attractive interactions. We observe the manifestation of modulational instability that, instead of causing collapse, fragments a large two-dimensional superfluid into multiple wave packets universally around a threshold atom number necessary for the formation of Townes solitons. We confirm that the density distributions of quench-induced solitary waves are in excellent agreement with the stationary Townes profiles. Furthermore, our density measurements in the space and time domain reveal detailed information about this dynamical process, from the hyperbolic growth of density waves, the formation of solitons, to the subsequent collision and collapse dynamics, demonstrating multiple universal behaviors in an attractive many-body system in association with the formation of a quasistationary state.

DOI: 10.1103/PhysRevLett.125.250401

Predicting the evolution of multidimensional nonlinear systems under attractive interactions is a challenging task, owing to the instability to collapse [1–3]. Bright solitons are remarkable stationary states, established when the self-focusing effect responsible for collapse is exactly compensated by wave dispersion [4,5]. In uniform two-dimensional (2D) systems with standard cubic interactions, such as Kerr medium [3,6] or matter waves formed by weakly interacting 2D Bose gases [7,8], however, such intricate balance cannot be fulfilled except when a wave packet possesses a critical norm (or total atom number) known as the Townes threshold and a specific waveform known as the Townes profile [6,9,10]—only at which bright solitons can form. A Townes soliton is predicted to be unstable as long as the norm deviates from the Townes threshold [3,9]. Despite extensive interest in multidimensional bright solitons [9–13], including recent advancements on 2D spatial solitons in various nonlinear optics settings [3,11,14], an experimental realization and characterization of Townes solitons has remained elusive.

In soliton formation dynamics, modulational instability (MI) is a ubiquitous mechanism that causes the amplification of initial wave disturbances and fragmentation into solitary waves [1,15–17]. In one-dimensional (1D) systems, MI is responsible for the formation of stable soliton trains, for example, in nonlinear fiber optics [18–20], in 1D Bose gases [16,17,21,22], or in Bose-Einstein condensates in optical lattices [23–25]. In higher spatial dimensions, transverse MI and wave fragmentation were studied in various types of bulk nonlinear optical media [14,26,27]. However, detailed dynamics of multidimensional MI and its possible connection to the universal formation of a quasistationary state, the unstable Townes solitons, have not been clearly demonstrated.

Using ultracold 2D Bose gases, we show that universal MI dynamics supports the critical formation of Townes solitons. Starting with a 2D superfluid of an initial density n_i and quenched to an attractive interaction $g_f < 0$, we show that MI causes collective modes with a wave number around $k_{\mathrm{MI}} = \pi/\xi$ associated with the interaction length $\xi = \pi/\sqrt{2n_i|g_f|}$ to grow predominantly [28–30], fragmenting the superfluid as illustrated in Fig. 1(a). Intriguingly, the characteristic atom number in each wave packet $\sim n_i\xi^2 = \pi^2/2|g_f|$ well approaches the Townes threshold $N_{\mathrm{th}} = 5.85/|g_f|$ [10], thus opening up a pathway for Townes soliton formation. This relation should apply universally for any n_i and g_f provided no other length scales set in. We note that, due to the scaling symmetry in 2D, a Townes soliton forms under a scale-invariant profile [6] and MI can set the physical length scale ξ that depends only on the product of n_i and $|g_f|$.

In this Letter, we report the observation of universal dynamics and Townes soliton formation in quenched 2D Bose gases. We observe MI that breaks up an otherwise large 2D sample into fragments universally around the Townes threshold. We clearly identify solitary waves whose density distributions agree well with the Townes profiles—the stationary state solution of the 2D nonlinear Schrödinger equation (NLSE) [6,10]. Our measurement further reveals universal solitary wave dynamics governed by the MI timescale and a universal scaling behavior in the density power spectra, allowing us to clearly identify a distinct time period for the unstable growth of density waves (while conserving

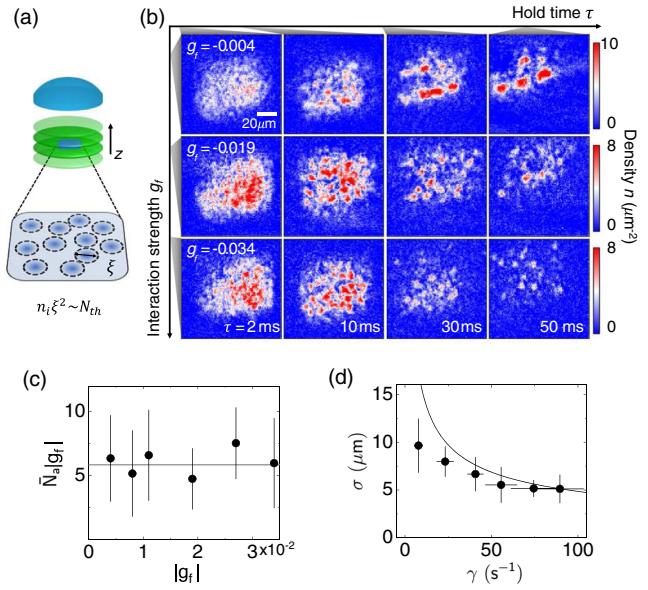

FIG. 1. Universal solitary wave formation in quenched 2D Bose gases. (a) Interaction quench-induced MI fragments a 2D gas (blue shaded square) into wave packets of a characteristic size ξ (dashed circles) that contains atom number $\sim n_i\xi^2$ approaching the Townes threshold $N_{\rm th}$. The 2D gas is confined in a single node of a repulsive standing-wave potential (green shaded ovals), evolves for a hold time τ, and is imaged via a microscope objective (blue hemisphere) [31]. (b) Single-shot images of samples quenched to the indicated interaction g_f (in each row) and held for the labeled time τ (in each column). Solitary waves (isolated density blobs) become visible at $\tau \geq 30$ ms. (c) Scaled mean atom number in a solitary wave $\bar{N}_a|g_f|$. Solid line marks the universal threshold $N_{\rm th}|g_f| = 5.85$. (d) Mean size σ versus interaction frequency γ. Solid line is the interaction length ξ. All data points in (c) and (d) are evaluated at $\tau = 42 \sim 50$ ms except for those of $g_f = -0.004$ which are evaluated at $\tau = 150 \sim 200$ ms. Error bars are standard errors. Uncertainties in g_f are smaller than the size of symbols [31].

total atom number), followed by a short era of wave collapse and soliton formation.

We begin the experiment with a uniform 2D Bose gas deep in the superfluid regime [31], which is formed by $N \approx 1.5 \times 10^4$ cesium atoms trapped inside a quasi-2D box potential. The atomic surface density is $n_i \approx 5/\mu{\rm m}^2$ and the surface area is controlled by a wall-like potential that is removed following the interaction quench [31]. The tight vertical (z) confinement of the box freezes all atoms in the harmonic ground state along z axis. The trap vibrational level spacing ($\omega_z = 2\pi \times 1750$ Hz) is more than 2 orders of magnitude larger than the attractive interaction energy studied, ensuring that the observed wave dynamics is effectively 2D [38]. The interaction strength $g = \sqrt{8\pi}a/l_z$ is controlled by the tunable s-wave scattering length a via a magnetic Feshbach resonance [39], and $l_z = 208$ nm is the vertical harmonic oscillator length; $g = g_i = 0.115$ is the initial interaction strength.

We perform an interaction quench (in 1 ms) to various $g = g_f$ in samples with a large surface area $A \approx (60\ \mu{\rm m})^2$. Following a variable hold time τ, we perform single-shot absorption imaging to record the sample density distribution as shown in Fig. 1(b). Around 30 samples are imaged for ensemble analyses. In a short hold time, we observe density blobs randomly clumping up throughout a sample. The sizes of the blobs are smaller with larger $|g_f|$. At a longer hold time, $\tau \geq 30$ ms, the number of observed blobs reduces, becoming more isolated, although the mean size and atom number of the surviving blobs remain nearly unchanged for $\tau \leq 200$ ms (see Fig. S2 in Ref. [31]). The same quench protocol applied to samples in a three-dimensional trap ($\omega_z \approx 2\pi \times 100$ Hz with a weak radial trap frequency $\omega_r \approx 2\pi \times 13$ Hz) results in no observed density blobs.

We characterize these isolated blobs (solitary waves) and compare their atom number with the Townes threshold. We approximate their density profiles by 2D Gaussians [10] and fit the mean size σ and atom number $\bar{N}_a$ [31]. Within the interaction range studied, $-0.004 \geq g_f \geq -0.034$, in Fig. 1(c) we find that all rescaled atom numbers $\bar{N}_a|g_f|$ fall around $N_{\rm th}|g_f| = 5.85$, giving a mean $\overline{\bar{N}_a|g_f|} = 6(1)$. Interestingly, the standard deviation of the atom number δN_a scales with g_f accordingly, giving a mean fluctuation $\overline{\delta N_a|g_f|} = 3.2(5) \sim 0.5\overline{\bar{N}_a|g_f|}$. We believe that the number variation around the threshold results from the energy-time uncertainty relation, as we later show that these blobs form in a timescale $\sim\gamma^{-1}$, where $\hbar\gamma = \hbar^2 n_i|g_f|/m$ is the interaction energy, m is the atomic mass, and $\hbar$ is the reduced Planck constant. Moreover, the size of these solitary waves also agrees with the prediction $\sigma \approx \xi$ in Fig. 1(d), indicating that MI provides the length scale for the formation of blobs. A size discrepancy at $\gamma \approx 2\pi \times 1.2$ Hz ($g_f = -0.004$) could likely be attributed to the influence of a very weak horizontal corrugation in the vertical confining potential.

To confirm that the quench-induced solitary waves indeed form Townes solitons, we compare their density distributions with the scale-invariant, isotropic Townes profile $n(r) = \alpha^2|\phi(\alpha r)|^2/(2|g_f|)$, where $\alpha = \sqrt{2n_0|g_f|/|\phi(0)|^2}$ is a scale factor. Given the peak density n_0, the characteristic size and density profile of a Townes soliton are uniquely determined. Here, the radial function $\phi(\tilde{r})$ is the stationary solution of the scale-invariant 2D NLSE [6,10]. The stationary profile $\phi(\tilde{r})$ has been evaluated numerically [6], giving $|\phi(0)| \approx 2.207$, and the norm $\int |\phi(\tilde{r})|^2 d\tilde{\mathbf{r}} \approx 11.7$ sets the Townes threshold.

Since MI sets the length scale during the soliton formation process, $\alpha \sim \xi^{-1}$, the peak density of most solitons should be comparable to the initial sample density $n_0 \approx n_i$. Figure 2 plots three isolated solitary waves of similar peak density that are randomly chosen from quenched samples ($g_f = -0.034$) at a long hold time

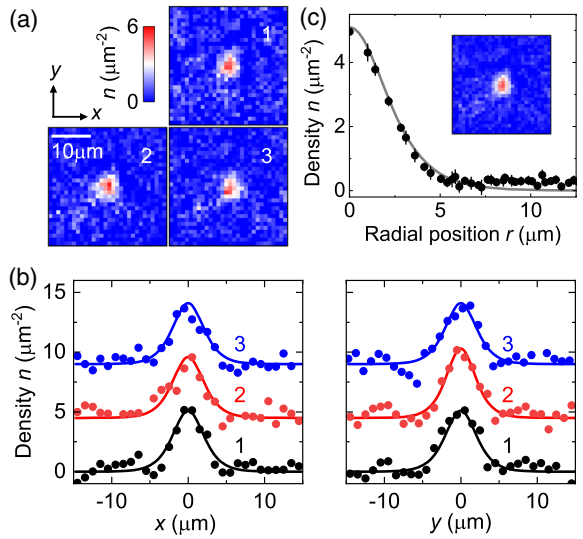

FIG. 2. Townes solitons and the Townes profiles. (a) Sample images of single solitary waves ($g_f = -0.034$) recorded at $\tau = 100$ ms. (b) Density line cuts (solid circles) through the center of images as numerically labeled in (a). Each data is offset by $4.5/\mu\text{m}^2$ for viewing. Solid lines are the Townes profiles of peak densities $n_0 = 5.1/\mu\text{m}^2$ (for #1, #3) and $5.8/\mu\text{m}^2$ (for #2), respectively. (c) Azimuthally averaged radial profile (solid circles) from the mean density image of (a) (inset: 30×30 μm^2), in close comparison with theory (solid curve) calculated using $n_0 = 5.1/\mu\text{m}^2$. Nearby dispersed blobs contribute to a small background at $r \gtrsim 7$ μm.

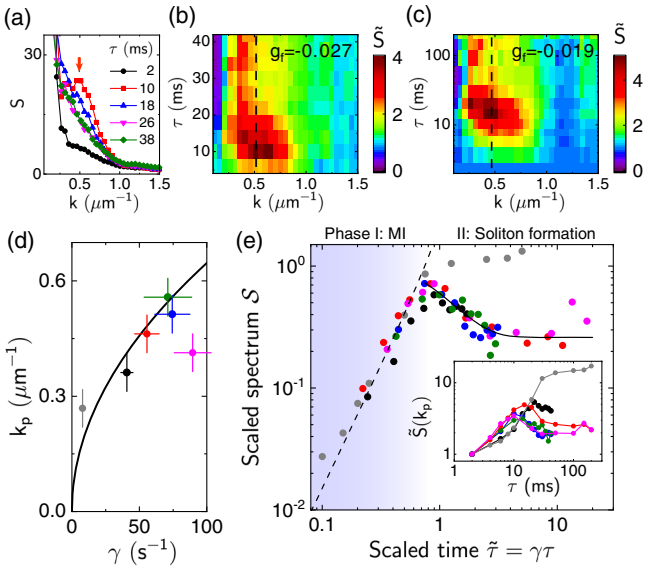

FIG. 3. Dynamics and universal scaling in the density power spectra. (a) Sample spectra $S(k,\tau)$ at $g_f = -0.027$ and the indicated hold time τ. (b) Corresponding growth spectra $\tilde{S}(k,\tau) = S(k,\tau)/S(k,\tau_0)$ with $\tau_0 = 2$ ms. (c) Sample growth spectra $\tilde{S}$ at $g_f = -0.019$ and hold time up to 200 ms. Vertical dashed lines in (b) and (c) mark the peak wave number k_p. (d) k_p versus interaction frequency γ (filled circles) measured at $g_f = -0.004$ (gray), -0.011 (black), -0.019 (red), -0.027 (blue), and -0.034 (magenta and olive), respectively. Corresponding $\tilde{S}(k_p,\tau)$ are shown in the inset of (e). Solid line is the prediction $k_{\text{MI}} = \sqrt{2\gamma m/\hbar}$. Error bars include systematic and statistical errors. (e) Scaled spectra $\mathcal{S}$ plotted using Eq. (1), which collapse approximately onto a single curve except for the one at $g_f = -0.004$. Dashed line (Solid line) is a hyperbolic (exponential) fit to Phase I, $\tilde{\tau} < 0.8$ (II, $\tilde{\tau} > 0.8$), of the collapsed spectra; see text.

$\tau = 100$ ms. Their individual density distributions, as well as the averaged radial density profile, indeed agree fairly well with the expected Townes profiles with no fitting parameters. More agreement with the Townes profiles is discussed in Ref. [31], where a single array of well-isolated solitons can form in an elongated sample following an interaction quench. Our observation confirms that Townes solitons can prevail from MI and explains why many randomly formed solitary waves, as observed in Fig. 1, are long-lived. We note that, in the absence of MI and fragmentation, a wave was observed to collapse only partially to a Townes profile [3].

We now turn to study the universal dynamics during the soliton formation process. We focus on the time evolution of density power spectrum [40] $S(k,\tau) = \langle |n(k,\tau)|^2 \rangle / N$ in the spatial frequency domain (momentum space), using the Fourier transform of the sample density distribution. Here $k = |\mathbf{k}|$ is the momentum wave number of the azimuthally averaged spectrum, N is the total atom number, and $\langle \cdots \rangle$ denotes ensemble averaging. In the power spectra [Fig. 3(a)], we clearly observe rapid growth of a nonzero momentum peak at short hold time (marked by an arrow), indicating the development of density waves at a dominant length scale throughout the sample. The nonzero momentum peak then dissipates at longer hold time until the power spectrum finally becomes monotonic and stationary, which signifies the collapse of density waves and fragmentation of the sample into solitons that later becomes uncorrelated in coordinate space.

The evidence of MI-induced wave amplification at different interaction strengths is best illustrated when we plot the relative growth spectra $\tilde{S}(k,\tau) = S(k,\tau)/S(k,\tau_0)$, normalized by the initial power spectrum at $\tau_0 = 2$ ms. This allows us to determine which mode has the largest growth rate. For different samples in Figs. 3(b) and 3(c), the momentum peak is clearly visible within $0.2/\mu\text{m} < k < 1/\mu\text{m}$ at short hold time. The growth patterns look similar for samples with different g_f, although the peak location, height, and the evolution timescale vary. We identify the peak wave number k_p and find consistency with the prediction from MI in Fig. 3(d).

Another remarkable prediction from MI is that, regardless of the dimensionality of the system, the power spectrum at k_p exhibits a universal time and amplitude scaling behavior with respect to the interaction timescale γ^{-1}. This is based on extending the Bogoliubov phonon picture to the regime under attractive interactions, which

predicts that collective modes of opposite momenta are generated in pairs, as seeded from initial density perturbations, and subsequently form density waves along the associative directions while being amplified at a rate γ until significant depletion of the ground state atoms occurs [31].

In Fig. 3(e), we experimentally test the scaling relation in the peak growth spectra $\tilde{S}(k_p, \tau)$, covering the entire time period. We summarize the scaling relation as follows:

$$\mathcal{S}(\tilde{\tau}) \approx \frac{\gamma}{\bar{\gamma}_i}[\tilde{S}(k_p, \tilde{\tau}) - 1], \tag{1}$$

where $\tilde{\tau} = \gamma\tau$ is the scaled time and $\mathcal{S}(\tilde{\tau})$ is the scaled spectrum. In the amplitude scaling, we normalize γ with the mean initial interaction energy unit $\bar{\gamma}_i = 306\ \mathrm{s}^{-1}$ before the quench [31]. We show that six power spectra, each with different γ, can collapse onto a single curve over a surprisingly long scaled time $\tilde{\tau} < 10$. The only exception is the spectrum at $g_f = -0.004$, where we have used $\gamma^* = 3.2\gamma$ to force its collapse within $\tilde{\tau} \leq 0.8$. This different behavior is likely due to a weak horizontal trap corrugation influencing the dynamics, as noted in Fig. 1(d).

From this universal spectrum, we identify two distinct regimes of dynamics, divided by a critical time $\tilde{\tau}_c \approx 0.8$ as shown in Fig. 3(e). We label the time period $\tilde{\tau} \leq \tilde{\tau}_c$ for MI with an amplified (hyperbolic) growth of density waves [31],

$$\tilde{S}(k_p, \tau) \approx 1 + \alpha\frac{\bar{\gamma}_i}{\gamma}\sinh^2(\gamma\tau), \tag{2}$$

where $\alpha = 1.5(1)$ is determined from a fit to $\mathcal{S}(\tilde{\tau})$ for $\tilde{\tau} \leq 0.5$; $\alpha = 2$ is obtained from the theory calculation for $\tilde{\tau} \ll 1$, neglecting the depletion of ground state atoms, dissipation, or interaction between the collective modes. Beyond $\tilde{\tau} \geq \tilde{\tau}_c$ after $\mathcal{S}(\tilde{\tau})$ reaches the order of unity, dynamics enters the second phase, decaying with a time constant $\Delta\tilde{\tau} \sim 0.8$ and transitioning to a slowly evolving, quasistationary behavior.

Our data suggest the existence of a universal time and amplitude scaling behavior and a limit for the amplified density wave, followed by a universal dynamics for the wave collapse and soliton formation. For $g_f = -0.004$, however, $\tilde{S}(k_p, \tau)$ remains slowly growing within $1 \leq \gamma^*\tau \leq 10$, suggesting a less severe wave collapse.

Following the observed density wave collapse dynamics, a 2D sample fragments into many solitary wave packets of characteristic size $\sigma \sim \xi$. As seen in Fig. 1, due to the close proximity of many wave packets (also with characteristic distances $\sim\xi$), collisions between them may induce collapses that lead to rapid atom number loss. Here, we show that the MI timescale continues to dominate the collision dynamics and the total atom number loss in a quenched 2D Bose gas.

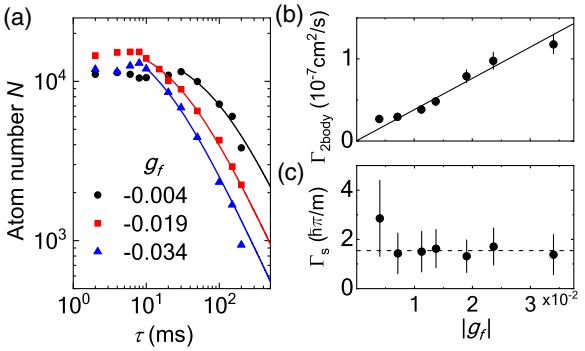

FIG. 4. Universal soliton collision dynamics in 2D. (a) Sample loss curves in total atom number N measured at the indicated interaction g_f. Solid lines are two-body loss fits after atom loss initiates. (b) Fitted rate coefficients. Solid line is a linear fit, giving a slope $\Gamma_{2\mathrm{body}}/|g_f| = 3.8(2) \times 10^{-6}\ \mathrm{cm}^2/\mathrm{s}$. (c) 2D soliton binary loss coefficients Γ_s determined from the rate coefficients in (b) and $\bar{N}_a$ as in Fig. 1(c), and compared with the universal prediction Eq. (3), giving a mean $\eta = 1.5(1)$ (dashed line) and agreeing with $\eta = 1.5(3)$ alternatively determined from the fitted slope in (b) and mean $\overline{\bar{N}_a|g_f|} = 6(1)$. Error bars are standard errors. Uncertainties in g_f are smaller than the size of symbols [31].

In a recent study of 1D soliton collisions [41], it is shown that merger occurs when solitons of similar phases collide, and two solitons of opposite phases appear to repel each other. In 2D, the merger of two solitonlike wave packets should lead to a new atom number $N_a > N_{\mathrm{th}}$. This can induce collapse that quickly removes the merged soliton. For solitons or density blobs formed by MI with randomly seeded density waves in a large 2D sample, one expects no fixed phase relationship between neighbors. Merger can thus occur randomly throughout the sample and the total atom number loss may reveal the scaling of soliton binary collision losses.

In Fig. 4, we examine the total atom number loss for the samples quenched to different g_f (Fig. 1). We observe the onset of loss in each sample at a time τ corresponding roughly to the critical time $\tilde{\tau}_c$, a behavior similarly observed for MI in 1D [16]. Beyond the critical time, we confirm that the loss curves can be well captured by a simple two-body loss model, $\dot{N}/N = -\Gamma_{2\mathrm{body}}N/A$. We attribute this behavior to the dominance of binary collisions between solitons or density blobs that trigger collapse and atom number loss; without triggered collapse, the usual three-body recombination loss should be negligible [42]. In Fig. 4(b), we find a linear dependence on $|g_f|$ in the measured loss coefficients $\Gamma_{2\mathrm{body}}$. This in fact suggests a constant binary loss coefficient Γ_s for colliding wave packets, where $\Gamma_s = \Gamma_{2\mathrm{body}}\bar{N}_a$ [31] and $\bar{N}_a|g_f| \approx 6$ is the measured universal number for solitary waves formed by MI.

We suspect this universal loss behavior results from MI scaling and 2D scale invariance, which suggests a constant binary loss coefficient,

$$\Gamma_s = \eta \frac{\hbar\pi}{m}, \tag{3}$$

independent of the interaction parameters (n_i, g_f). This is because the collision rate $\Gamma_s \sim \sigma\bar{v}$ and the dependences on length scales in the linear cross section $\sigma \approx \xi$ and relative velocity $\bar{v} \approx \sqrt{2}\hbar\pi/m\xi$ cancel each other; the constant $\eta \approx \sqrt{2}$ is estimated for ~50% probability of merger per collision or, equivalently, on average one soliton or density-blob loss per collision event. If Eq. (3) holds, we expect a collision lifetime $1/n_s\Gamma_s \sim \gamma^{-1}$, where $n_s = n_i/\bar{N}_a$ is the initial soliton/blob density [31]. This suggests that wave collapse and binary collision likely take place at the same rate during the second phase of the density evolution.

To unambiguously confirm the universality of collision dynamics, in Fig. 4(c) we deduce Γ_s independently using experimentally determined values $(\Gamma_{2\text{body}}, \bar{N}_a)$ at each g_f. Our results conform very well with the prediction by Eq. (3), giving a mean $\eta \approx 1.5$. We emphasize here that the loss coefficients universally depend only on the physical constants $\hbar/m$ is a remarkable manifestation of MI and scale-invariant symmetry in 2D. The observations in Figs. 3 and 4 together confirm that interaction quench dynamics leads to Townes soliton formation at $\tau \gtrsim \gamma^{-1}$, followed by collision (that induces collapse) also at the same timescale γ^{-1} universally governed by MI.

In summary, we study the universal nonequilibrium dynamics in degenerate 2D Bose gases quenched from repulsive to attractive interactions, and observe the dynamical formation of Townes solitons from MI. Townes solitons are observed to be collisionally unstable. However, further stabilization and manipulation may be possible [11,43–45]. We note that the initial shape and finite sample size can be further manipulated to invoke strong boundary effects in quench-induced MI [31]. Using slow interaction ramps may also induce MI dynamics deviating from the reported universal behavior. Soliton formation may be disrupted, leading to, for example, only partial collapse to the Townes profiles [3]. Lastly, we comment that controlled formation of 2D solitons via pair-production processes in MI may find future applications in matter-wave interferometry [46,47], or even in the generation and distribution of many-body entanglement [48–51].

We acknowledge discussions with Qi Zhou, Chih-Chun Chien, Sergei Khlebnikov, and Chris Greene. We thank Cheng Chin for discussions and many critical comments. We are grateful to H. J. Kimble for instrument loan since the early stage of this project. We thank May Kim, Yiyang Fang, and Wuxiucheng Wang for laboratory assistance. This project is supported in part by the Purdue Research Foundation, the W. M. Keck Foundation, the NSF Grant No. PHY-1848316, and the U.S. Department of Energy (Grant No. DE-SC0019202).

*clhung@purdue.edu

[1] P. A. Robinson, Nonlinear wave collapse and strong turbulence, Rev. Mod. Phys. **69**, 507 (1997).
[2] E. A. Donley, N. R. Claussen, S. L. Cornish, J. L. Roberts, E. A. Cornell, and C. E. Wieman, Dynamics of collapsing and exploding Bose–Einstein condensates, Nature (London) **412**, 295 (2001).
[3] K. D. Moll, A. L. Gaeta, and G. Fibich, Self-Similar Optical Wave Collapse: Observation of the Townes Profile, Phys. Rev. Lett. **90**, 203902 (2003).
[4] N. J. Zabusky and M. D. Kruskal, Interaction of "Solitons" in a Collisionless Plasma and the Recurrence of Initial States, Phys. Rev. Lett. **15**, 240 (1965).
[5] V. F. Zakharov and A. B. Shabat, Exact theory of two-dimensional self-focusing and one-dimensional self-modulation of waves in nonlinear media, Sov. Phys. JETP **34**, 62 (1972).
[6] R. Y. Chiao, E. Garmire, and C. H. Townes, Self-Trapping of Optical Beams, Phys. Rev. Lett. **13**, 479 (1964).
[7] L. Chomaz, L. Corman, T. Bienaimé, R. Desbuquois, C. Weitenberg, S. Nascimbène, J. Beugnon, and J. Dalibard, Emergence of coherence via transverse condensation in a uniform quasi-two-dimensional bose gas, Nat. Commun. **6**, 6162 (2015).
[8] C.-L. Hung, X. Zhang, N. Gemelke, and C. Chin, Observation of scale invariance and universality in two-dimensional Bose gases, Nature (London) **470**, 236 (2011).
[9] Y. V. Kartashov, B. A. Malomed, and L. Torner, Solitons in nonlinear lattices, Rev. Mod. Phys. **83**, 247 (2011).
[10] B. A. Malomed, Multidimensional solitons: Well-established results and novel findings, Eur. Phys. J. Spec. Top. **225**, 2507 (2016).
[11] J. W. Fleischer, M. Segev, N. K. Efremidis, and D. N. Christodoulides, Observation of two-dimensional discrete solitons in optically induced nonlinear photonic lattices, Nature (London) **422**, 147 (2003).
[12] S. L. Cornish, S. T. Thompson, and C. E. Wieman, Formation of Bright Matter-Wave Solitons During the Collapse of Attractive Bose-Einstein Condensates, Phys. Rev. Lett. **96**, 170401 (2006).
[13] Y. V. Kartashov, G. E. Astrakharchik, B. A. Malomed, and L. Torner, Frontiers in multidimensional self-trapping of nonlinear fields and matter, Nat. Rev. Phys. **1**, 185 (2019).
[14] Z. Chen, M. Segev, and D. N. Christodoulides, Optical spatial solitons: Historical overview and recent advances, Rep. Prog. Phys. **75**, 086401 (2012).
[15] V. E. Zakharov and L. Ostrovsky, Modulation instability: The beginning, Physica (Amsterdam) **238D**, 540 (2009).
[16] J. H. Nguyen, D. Luo, and R. G. Hulet, Formation of matter-wave soliton trains by modulational instability, Science **356**, 422 (2017).
[17] P. J. Everitt, M. A. Sooriyabandara, M. Guasoni, P. B. Wigley, C. H. Wei, G. D. McDonald, K. S. Hardman, P. Manju, J. D. Close, C. C. N. Kuhn, S. S. Szigeti, Y. S. Kivshar, and N. P. Robins, Observation of a modulational instability in Bose-Einstein condensates, Phys. Rev. A **96**, 041601(R) (2017).
[18] K. Tai, A. Hasegawa, and A. Tomita, Observation of Modulational Instability in Optical Fibers, Phys. Rev. Lett. **56**, 135 (1986).

[19] D. Solli, G. Herink, B. Jalali, and C. Ropers, Fluctuations and correlations in modulation instability, Nat. Photonics **6**, 463 (2012).
[20] J. M. Dudley, F. Dias, M. Erkintalo, and G. Genty, Instabilities, breathers and rogue waves in optics, Nat. Photonics **8**, 755 (2014).
[21] K. E. Strecker, G. B. Partridge, A. G. Truscott, and R. G. Hulet, Formation and propagation of matter-wave soliton trains, Nature (London) **417**, 150 (2002).
[22] L. Khaykovich, F. Schreck, G. Ferrari, T. Bourdel, J. Cubizolles, L. D. Carr, Y. Castin, and C. Salomon, Formation of a matter-wave bright soliton, Science **296**, 1290 (2002).
[23] V. V. Konotop and M. Salerno, Modulational instability in Bose-Einstein condensates in optical lattices, Phys. Rev. A **65**, 021602(R) (2002).
[24] I. Carusotto, D. Embriaco, and G. C. La Rocca, Nonlinear atom optics and bright-gap-soliton generation in finite optical lattices, Phys. Rev. A **65**, 053611 (2002).
[25] O. Morsch and M. Oberthaler, Dynamics of Bose-Einstein condensates in optical lattices, Rev. Mod. Phys. **78**, 179 (2006).
[26] A. V. Mamaev, M. Saffman, D. Z. Anderson, and A. A. Zozulya, Propagation of light beams in anisotropic nonlinear media: From symmetry breaking to spatial turbulence, Phys. Rev. A **54**, 870 (1996).
[27] Y. S. Kivshar and D. E. Pelinovsky, Self-focusing and transverse instabilities of solitary waves, Phys. Rep. **331**, 117 (2000).
[28] L. Salasnich, A. Parola, and L. Reatto, Modulational Instability and Complex Dynamics of Confined Matter-Wave Solitons, Phys. Rev. Lett. **91**, 080405 (2003).
[29] L. D. Carr and J. Brand, Spontaneous Soliton Formation and Modulational Instability in Bose-Einstein Condensates, Phys. Rev. Lett. **92**, 040401 (2004).
[30] A. H. Guth, M. P. Hertzberg, and C. Prescod-Weinstein, Do dark matter axions form a condensate with long-range correlation? Phys. Rev. D **92**, 103513 (2015).
[31] See Supplemental Material at http://link.aps.org/supplemental/10.1103/PhysRevLett.125.250401 for detailed experiment procedures, theory derivations, and supplemental measurements, which includes Refs. [32–37].
[32] C.-L. Hung, X. Zhang, L.-C. Ha, S.-K. Tung, N. Gemelke, and C. Chin, Extracting density–density correlations from in situ images of atomic quantum gases, New J. Phys. **13**, 075019 (2011).
[33] L. Feng, L. W. Clark, A. Gaj, and C. Chin, Coherent inflationary dynamics for Bose–Einstein condensates crossing a quantum critical point, Nat. Phys. **14**, 269 (2018).
[34] L. Pitaevskii and S. Stringari, *Bose-Einstein Condensation and Superfluidity* (Oxford University Press, New York, 2016), Vol. 164.
[35] Y. Kagan, A. E. Muryshev, and G. V. Shlyapnikov, Collapse and Bose-Einstein Condensation in a Trapped Bose Gas with Negative Scattering Length, Phys. Rev. Lett. **81**, 933 (1998).
[36] H. Saito and M. Ueda, Intermittent Implosion and Pattern Formation of Trapped Bose-Einstein Condensates with an Attractive Interaction, Phys. Rev. Lett. **86**, 1406 (2001).
[37] H. Saito and M. Ueda, Mean-field analysis of collapsing and exploding Bose-Einstein condensates, Phys. Rev. A **65**, 033624 (2002).
[38] P. Pedri and L. Santos, Two-Dimensional Bright Solitons in Dipolar Bose-Einstein Condensates, Phys. Rev. Lett. **95**, 200404 (2005).
[39] C. Chin, R. Grimm, P. Julienne, and E. Tiesinga, Feshbach resonances in ultracold gases, Rev. Mod. Phys. **82**, 1225 (2010).
[40] C.-L. Hung, V. Gurarie, and C. Chin, From cosmology to cold atoms: Observation of sakharov oscillations in a quenched atomic superfluid, Science **341**, 1213 (2013).
[41] J. H. Nguyen, P. Dyke, D. Luo, B. A. Malomed, and R. G. Hulet, Collisions of matter-wave solitons, Nat. Phys. **10**, 918 (2014).
[42] T. Kraemer, M. Mark, P. Waldburger, J. G. Danzl, C. Chin, B. Engeser, A. D. Lange, K. Pilch, A. Jaakkola, H.-C. Nägerl *et al.*, Evidence for Efimov quantum states in an ultracold gas of caesium atoms, Nature (London) **440**, 315 (2006).
[43] H. Saito and M. Ueda, Dynamically Stabilized Bright Solitons in a Two-Dimensional Bose-Einstein Condensate, Phys. Rev. Lett. **90**, 040403 (2003).
[44] N. K. Efremidis, J. Hudock, D. N. Christodoulides, J. W. Fleischer, O. Cohen, and M. Segev, Two-Dimensional Optical Lattice Solitons, Phys. Rev. Lett. **91**, 213906 (2003).
[45] B. B. Baizakov, B. A. Malomed, and M. Salerno, Multidimensional solitons in a low-dimensional periodic potential, Phys. Rev. A **70**, 053613 (2004).
[46] A. D. Cronin, J. Schmiedmayer, and D. E. Pritchard, Optics and interferometry with atoms and molecules, Rev. Mod. Phys. **81**, 1051 (2009).
[47] B. Lücke, M. Scherer, J. Kruse, L. Pezzé, F. Deuretzbacher, P. Hyllus, J. Peise, W. Ertmer, J. Arlt, L. Santos *et al.*, Twin matter waves for interferometry beyond the classical limit, Science **334**, 773 (2011).
[48] K. Lange, J. Peise, B. Lücke, I. Kruse, G. Vitagliano, I. Apellaniz, M. Kleinmann, G. Tóth, and C. Klempt, Entanglement between two spatially separated atomic modes, Science **360**, 416 (2018).
[49] P. Kunkel, M. Prüfer, H. Strobel, D. Linnemann, A. Frölian, T. Gasenzer, M. Gärttner, and M. K. Oberthaler, Spatially distributed multipartite entanglement enables EPR steering of atomic clouds, Science **360**, 413 (2018).
[50] M. Fadel, T. Zibold, B. Décamps, and P. Treutlein, Spatial entanglement patterns and Einstein-Podolsky-Rosen steering in Bose-Einstein condensates, Science **360**, 409 (2018).
[51] D. Shin, B. Henson, S. Hodgman, T. Wasak, J. Chwedeńczuk, and A. Truscott, Bell correlations between spatially separated pairs of atoms, Nat. Commun. **10**, 4447 (2019).